Synthesis of Ag-doped TiO$_2$/MWCNT for DSSC application

M. MUJAHID[1,*], MOHAMMAD AHMAD[2], OMAR A. AL-HARTOMY[3]
[1]Physics Section, SHSSSB, Aligarh Muslim University Aligarh, U.P. 202002, India
[2]College of Nursing, King Saud University, Riyadh, Kingdom of Saudi Arabia
[3]Department of Physics, Faculty of Science, King Abdulaziz University, 21589, Jeddah, Saudi Arabia

The low-cost hydrothermal process can synthesize TiO$_2$/MWCNT with different doping concentrations of Ag. Synthesized substances were investigated by advanced electrical and spectroscopic methods like XRD, UV-vis, Photo Luminescence (P.L.), and Raman spectroscopy. The x-ray diffraction investigation revealed the crystallographic phase of TiO$_2$/MWCNT, remain unchanged by doping TiO$_2$ with different molar ratios of Ag. The morphology of TiO$_2$ was examined by TEM, which suggested the shape of the particle is spherical, and it was agglomerated over the surface of MWCNT. The mean particle size of titanium dioxide was found to be 25 nm. The UV-vis analysis confirmed the red shifting of Ag-doped TiO$_2$. This could be due to the surface plasmonic phenomena of Ag nanoparticles. P.L. spectra reveal two peaks at 360 nm (U.V. regime) and 480 nm (blue/green) regimes. These peaks are attributed to the intrinsic defects in the titanium dioxide crystal. Additionally, MWCNT enhances electron mobility on the working electrode side. Various electrical techniques examined the performance of the cell. DSSC synthesized under such conditions shows an increase in photocurrent density resulting in a 6.95% improvement in the conversion efficiency. The interfacial charge transfer phenomena of DSSC were also studied using Electrochemical Impedance Spectroscopy (EIS) analysis. The internal resistance of the cell is found to be 22 ohms. The efficiency of our synthesized solar cell is stable and eventually contributes up to 1000h of its use.

1. Introduction

The Dye-Sensitized Solar Cell, DSSC, is considered a new-generation solar cell. It is a clean energy source helpful in the sustainable development of human society [1]. It is used in windows or as wearable electronic products [2]. It is an electrolyte cell containing a positive counter electrode, Ag-doped TiO$_2$/MWCNT as the working electrode, dye molecule, and electrolyte. The performance of DSSC depends upon various structural parameters like harvesting more light, chemical stability in solution, and reducing the impedance of solar cells.

Titanium dioxide (TiO$_2$) is non-toxic, chemically stable against photocorrosion [3], environmentally friendly, and above all, it is a semiconductor of n-type interface material having an energy gap of 3.2 eV [4]. Doping of TiO$_2$/MWCNT with different concentrations of Ag nanoparticle favors its photocatalytic behavior in the visible spectrum of electromagnetic radiation [5]. Silver show significant contribution against visible light absorption and excellent charge transfer [6].

The first publication concerning doping of TiO$_2$ with noble metal was reported in 1978 by Tauster et al. [7]. After that, many kinds of research were written about the synthesis of Ag-doped TiO$_2$/MWCNT [8-9]. In 2014, Hyun-Jun Hwang and Hak-Sung Kim reported the synthesis of TiO$_2$/ silver/ carbon nanotube composite as photoanodic materials for DSSC. They observed the solar cell efficiency to be 3.76% [10]. In 2019, Yong Xiang Dong et al. observed the efficiency of DSSC using silver nanoparticles modified photoanode to be 5.05% [11]. Still, much research is ongoing to enhance the performance of DSSC.

This manuscript aims to synthesize TiO$_2$/MWCNT with different doping concentrations of Ag and its possible use in the fabrication of DSSC. We have carried out a detailed experiment to show the effect of doping on modifying photoanode that eventually contributes to the efficiency of the DSSC. Additionally, the structural, optical, electrical, and photoresponse of DSSC are investigated rationally. This study will benefit the development of panel displays, power windows, glass tiles, and many nanostructured-based devices.

The light conversion efficiency of DSSC has a significant correlation with specific electrical parameters like open-circuit voltage, V$_{oc}$, photoelectric current, and fill factor, FF. The evolution of stability and reproducibility of fabricated solar cells is also a key factor for upscaling and commercializing DSSC since it depends on the specific degradation technique [12]. Recently, Gabriela et al. [13] used Ruthenium dye and cobalt-based-polymer gel to investigate the improved performance and long stability of DSSC. They found that after 1000h efficiency of Ruthenium-based dye is statistically the same as a cobalt-based-polymer gel [13]. Mazumdar and his co-authors have used numerous working methods to stop degradation

and applied various deactivation methods to improve performance. This group observed that the cell's performance depends on different molar ratios and thicknesses [14]. Jan Luckas et al. have demonstrated a cheaper, durable method to increase the cohesion of DSSC by preventing the leakage, evaporation, and desorption of sensitized dye [15]. Following the reported result based on a similar concept, we use hermetic sealing strategies to extend the stability and reproducibility of DSSC [12-15].

2. Experimental techniques

2.1. Chemicals and Reagents

m-chloroperoxybenzoic acid (m-CPBA), MWCNT powder, chloroplatinic acid, Titaniumoxysulphate hydrate, silver nitrate, and bis-tetra-butylammonium were purchased from Aldrich-Sigma Company. Phenyl, octyl phenol ethylene oxide and 2-propanol, ethyl alcohol, methane carboxylic acid, and hydrogen sulfate were obtained from another Company (Merc Chemicals). All the reagents purchased from these two companies were of analytical grade.

2.2. Structure of DSSC

The DSSC consists of two translucent materials working as conducting and counter electrodes, Silver doped TiO_2 having MWCNT as support, the dye molecule, separator, and the liquid electrolyte (Fig. 1).

2.2.1. Translucent materials for both working and counter electrode

Khalil Jasim found that the optical transparency in conductive electrodes reduces after being coated with nanostructured material [12]. Following this observation, we used an FTO glass of constant thickness of 18 μm throughout the experiment, covered on its conductive side at the photoanode. In contrast, another glass plate coated with platinum was used as the counter electrode.

2.2.2. Nanostructured photoelectrode

TiO_2 provides high thermodynamic stability to the cell by improving cell anti-photocorrosion resistance [13]. The doping of TiO_2 with different concentrations of Ag enhances the roughness factor of the sensitized photoelectrode [12]. For synthesizing DSSC, the prepared paste of Ag-doped TiO_2/MWCNT was pasted on the conducting side of the FTO glass plate.

2.2.3 Photosensitizer

As reported earlier, we used Ruthenium dye N719, which extends the DSSC stability. N719 dye increases electrostatic binding onto the surface of the TiO_2 [16].

2.2.4. Redox electrolyte

The liquid electrolyte used in the synthesis of DSSC is iodide/triiodide (I^-/I_3^-) redox ions. This electrolyte can quickly transfer electrons between photoanode and counter electrodes [17].

2.3. Working principle of DSSC

The working principle of DSSC can be explained with the help of Fig. 1. Photosensitizer absorbs electrons when light is incident on it. Now, these electrons are transferred into the upper bands, called the conduction band of TiO_2. The liquid electrolyte I^-/I_3^- couple helps the electrons to return to the dye through the external load. This movement of electrons creates a current.
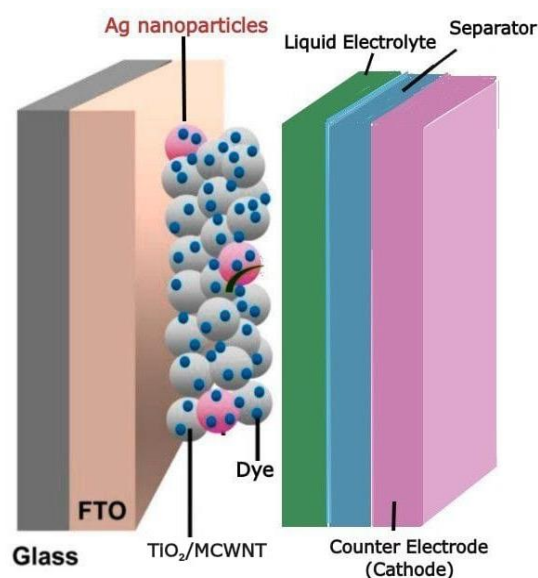
Fig. 1. Schematic working representation of DSSC (color online)

3. Synthesis of DSSC

3.1. Synthesis of Ag-TiO₂-MWCNT nanocomposite using hydrothermal process

The hydrothermal process is a cheaper synthesis process for finding the purest crystal quickly and at a justified temperature.

The hydrothermal process is realized when 3 g of MWCNT powder is heated with 5 g of m-CPBA in 200 ml of benzene at 180 °C for 20 h, continuously cooling the vapor produced back into the liquid. The semi-solid material so obtained was centrifuged in a beaker. The residual materials obtained were washed many times with double distilled water and ethanol. The obtained materials will be dried at 80 °C for 10 h in a dryer. In the whole

process, The MWCNT gets oxidized. In another beaker, 2g of titanium oxysulfate hydrate is heated with 200 ml of methane carboxylic acid, and 3 g of octyl phenol ethylene oxide (acting as a surfactant) is prepared in 200 ml of ethyl alcohol. The solution is prepared in 500 ml of water. The complete solution is centrifugated in a beaker. After that, 30 ml of concentrated hydrogen sulfate was added drop-wise into the solution with regular stirring by a magnet at 50 °C for 10 h.

The hydrothermal process was carried out by mixing MWCNT with the solution described above at 180 °C for 20 h. Combining the new solution is again carried out by heating the solution for about 5 h. This is followed by cooling the solution to room temperature. The residue obtained was filtered, washed with double distilled water and ethanol, followed by air-dried, and then calcinated at 400 °C for 16 h in a nitrogen atmosphere. For doping of Ag onto TiO_2, different concentrations (0.27 M, 0.46 M, 0.64 M, and 0.102 M) of $AgNO_3$ were added drop-wise in the surfactant solution.

3.2. Synthesis of solar cell assembly

For fabrication of DSSC, the residual mixture of synthesized material was mixed with 0.035M dilute ethanoic acid and 2-3 drops of octyl phenol ethylene oxide to prepare a paste. The synthesized material was then coated on the translucent side of the FTO glass plate (obtained from Asahi national glass company, New Delhi) thickness of 18 μm to ensure high optical transparency, stability, and reproducibility [12]. After coating, FTO glass was heated at 400 °C for about 50 minutes, and then residual materials were allowed to cool at room temperature to remove thermal stress. The FTO glass plate served as a working electrode, which was then immersed in a 0.5mM ethanol solution and bis-tetra-butylammonium dye for 5h. The counter electrode (cathode) was prepared by depositing platinum on the conducting side, followed by drying at 400 °C for 24 h. Hot melt foils sealed the cathodic and anodic plates to avoid solvent leakage, desorption, and evaporation. Then liquid electrolyte was poured into the cell. These steps were necessary for reproducibility and stability. A solar light (ORIEL) of power 1000W, model number 91192, was used to irradiate our synthesized solar cell. The intensity of the standard solar radiator was 100 mW/cm^2.

3.3. Characterization equipment

The XRD of synthesized materials TiO_2/MWCNT was investigated in the 2 theta range of 20-90 degrees with CuK_α radiations having wavelength λ = 0.15418 nm. The operating potential and current of the XRD beam were 30 kV and 15 mA, respectively. The UV-vis spectra were recorded using a Jasco V-770 spectrophotometer. Transmission electron microscopy was carried out using TEM, JEOL 3010 apparatus. Raman spectra were recorded using a Ui tech Raman spectrometer, which uses a green 532 nm laser light. P.L. spectra were investigated using a

He-Cd laser. V-I characteristic was measured using Keithley meter of modal number 2611A, while IPCE measurement was carried out using a multimeter, model number, PEC S-20.

4. Analysis of the results

4.1. Investigation of the result obtained from the XRD

XRD of TiO_2/MWCNT with distinct doping concentrations of Ag calcinated in the muffle furnace at a temperature of 400 °C for 16 h was analyzed and shown in Fig. 1. This figure reflects the crystalline phase of synthesized nanoparticles. The peaks attributed to the anatase phase of titanium dioxide with space group 141. The anatase phase network structure of TiO_2 is a good choice for adsorbing N-719 dye [13]. The XRD spectrum contains six diffraction peaks situated at 24.2, 35.0, 48.0, 65.0, 75.0, and 85.0 degrees at angle 2 theta (JCPD card number 21-1272). These peaks correspond to diffraction planes of (101), (004), (200), (105), (118), and (116). With increasing Ag doping, the diffraction peaks remain constant. This result illustrates that the anatase crystalline phase of TiO_2 remains constant with the doping of Ag. Only peak intensity increases with increasing doping concentrations. When a silver ion is combined with a regular and repeated pattern of TiO_2, a stretch is developed into the system, resulting in a modification in the pattern, decreasing the periodicity [18]. Qi et al. and Lee et al. reported that MWCNT was not harmed even after scorching [19-20], respectively. The stability of the synthesized solar cell was found to be the same as the reported results of Hyun-Jun [21].
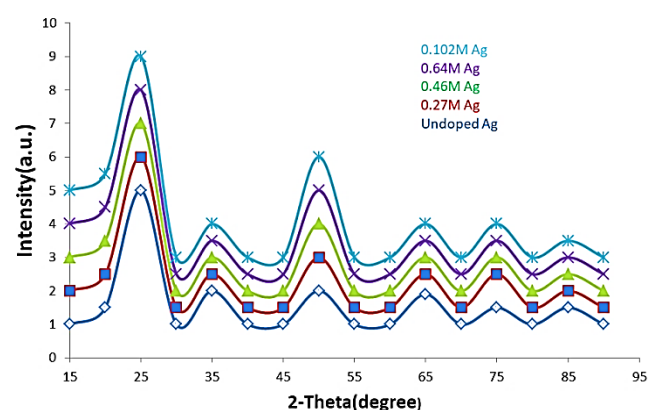
Fig. 2. XRD patterns of (a) TiO$_2$/MWCNT (b) 0.27 M Ag (c) 0.46 M Ag (d) 0.64 M Ag (e) 0.102 M Ag. Calcination temp: 400 ^{0}C, time of calcination: 16 h (color online)

The mean anatase crystallite size of TiO_2 was estimated with the help of results derived from Scherrer (15).

$$d_{hkl}= 0.9\lambda/\beta\cos\theta \qquad (1)$$

d_{hkl} is the crystallite size, Θ is the diffraction angle, and β is full width at half maxima. The crystallite size was calculated using equation (1) corresponding to diffraction peak (101) and found to be 25±1 nm. Thus, we find that the present morphology of TiO₂ has a valuable contribution to its photovoltaic effects [22].

4.2. UV-visible Spectra

The UV-vis spectrum of TiO₂/MWCNT samples doped with distinct engrossment of Ag was depicted in Fig. 2. Tangent drawn on absorption spectra intercepts on the x-axis is defined as absorption edge, which was found to shift from U.V. to the visible side. V. Stengl et al. explained this observation in the case of doping of La and Eu (rare earth metals) with TiO₂ [23-24]. The crystallite size and crystal spacing of synthesized material TiO₂/MWCNT with different concentrations of Ag were estimated using equation (2). The calculated results are illustrated in Table 1.

$$\lambda =2d\sin\Theta \qquad (2)$$

λ is the wavelength of light, Θ is the Bragg angle.

Table 1. Crystallite size of Ag-doped TiO₂/MWCNT with different concentrations of Ag. Calcination temp: 400 ⁰C, time of calcination: 16 h

Serial no.	Dopant engrossment (%)	Crystallite size (nm)	Crystal spacing (d) (nm)
1.	0	25±1	0.64
2.	0.27 M	20±1	0.54
3.	0.46 M	19±1	0.46
4.	0.64 M	18±1	0.42
5.	0.102 M	19±1	0.38

The corresponding E_g values were studied for undoped and doped samples using equation (3)

$$E_g=hc/\lambda \qquad (3)$$

where the value Planck's constant, h is 6.634×10^{-34} Js, and velocity of light c is 3×10^{8} m/s were given by 3.2 eV, 3.1 eV, 2.8 eV, 2.6 eV and 2.7 eV respectively. Thus the E_g values of Ag-doped TiO₂/MWCNT composite materials were lower in energy than undoped material. Reduction in the energy band of Ag-doped TiO₂/MWCNT material favors photovoltaic action under solar light irradiation [25]. We also find that the decrement of E_g value is found with the doping up to 0.64 M of Ag. The E_g values increase at higher dopant concentration (0.102 M Ag).

With the increase of doping, a continuum state which behaves like a band increases, increasing the bandgap.
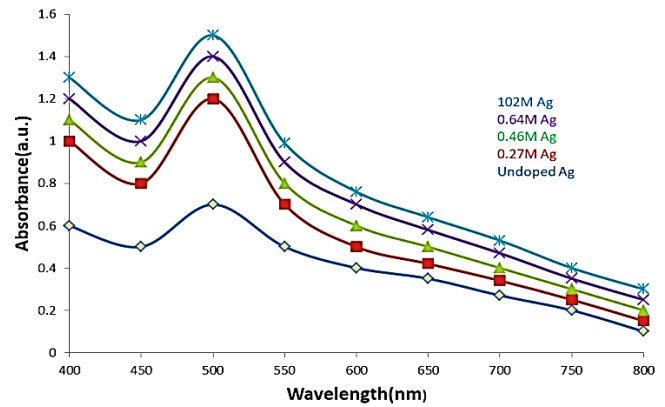
Fig. 3. Absorption spectra of (a) TiO₂/MWCNT (b) 0.27 M Ag (c) 0.46 M Ag (d) 0.64 M Ag (e) 0.102 M Ag. Calcination temp: 400 ⁰C, time of calcination: 16 h (color online)

4.3. TEM Analysis

The particle size, shape, and surface morphology were further examined by TEM. Fig. 4(a)-(d) shows TEM images of samples doped with 0.27 M, 0.46 M, 0.64 M, and 0.102 M of Ag onto TiO₂/ MWCNT composite material. Fig. 5 shows that the mean dimension of synthesized TiO₂ nanoparticles was found to be 25 nm. Calculated results with TEM were found to be more amicable than the result obtained using the Scherrer formula. Both XRD and TEM collectively gave valuable results about synthesized nanoparticles' morphology and particle size. We also find black-gray spherical particles seem to be agglomerated (Fig. 4(b)-(d)), confirming the doping of Ag onto TiO₂/MWCNT material. Thus, there is a close and deep association between doped Ag nanoparticles and undoped TiO₂/MWCNT. It is also clear from TEM analysis that the morphology of the spherical shape of TiO₂ nanoparticles could not change after the loading of different concentrations of silver nanoparticles onto TiO₂/ MWCNT composite material.

4.4. SAED analysis

Fig. 6 depicts the spectrum of Ag-doped TiO₂/MWCNT obtained with the help of the SAED apparatus. This pattern was taken during TEM imaging. Beam potential during TEM investigation was 200 kV. Fig. 6 also reveals concentric Debye rings corresponding to diffraction planes of (101), (004), (200), and (105); TEM results are incompatible with the results obtained from XRD.
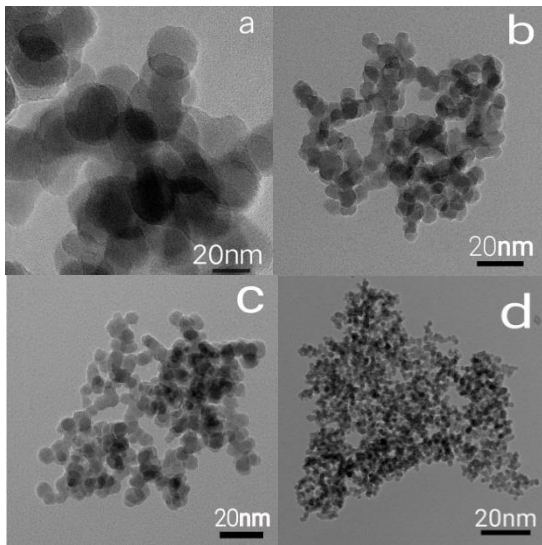
Fig. 4. TEM images of (a) 0.27 M Ag (b) 0.46 M Ag (c) 0.64 M Ag (d) 0.102 M Ag, calcination temp: 400 ^{0}C, time of calcination: 16 h
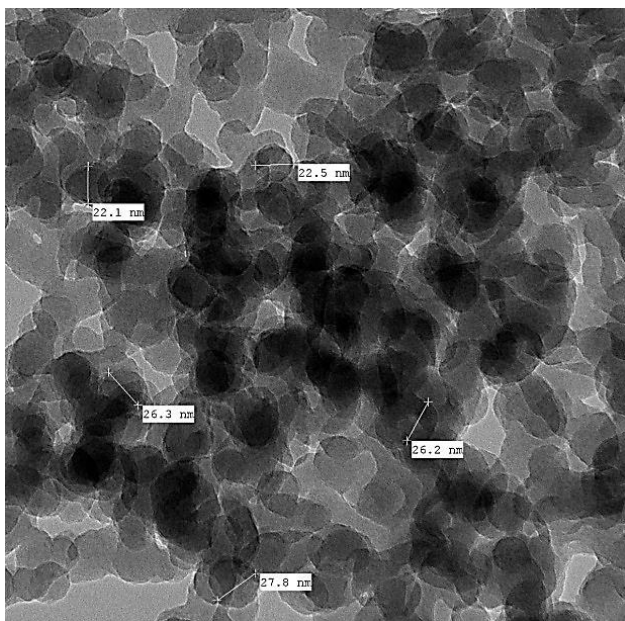
Fig. 5. TEM image of one of the samples doped with 0.46 M of Ag onto TiO$_2$/MWCNT. The mean particle size is found to be 25 nm. Calcination temp: 400 ^{0}C, time of calcination: 16 h

4.5. Raman spectra

Raman spectra provide identification of amorphous and crystalline phases. Raman scattering is an inelastic scattering consisting of Stokes and anti-Stokes lines. Raman scattering is considered an excitation of the molecules to a virtual state with energy lower in energy than an actual electronic transition, with a coincident de-excitation followed by a change in the vibrational energy. In the Raman spectrometer, the laser light is incident on

the sample to investigate. Fig. 7 provides the Raman spectra of undoped and one of the samples doped with 0.46 M of Ag onto TiO$_2$/MWCNT. We find a peak at 465 cm^{-1}, owing to the electro-optic mode of the anatase structure of TiO$_2$. We also find other line at 335 cm^{-1}, 380 cm^{-1}, 570 cm^{-1} and 620 cm^{-1}. They were related to B1$_g$, A1$_g$, E$_g$ (1), and E$_g$ (2) transition due to the anatase phase structure of TiO$_2$, respectively. The position of peaks of the Raman signal remains the same after doping with Ag, pointing to no phase transition. Peak intensity increases with the doping of different concentrations of Ag over TiO$_2$/MWCNT due to a decrease in the crystallite size and the bandgap, affecting the vibrational amplitude of the sample. These findings are according to the reported observations of Wang et al. [26].
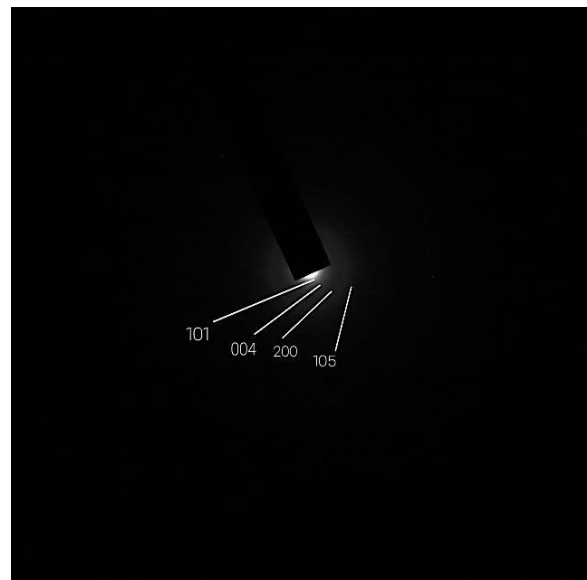
Fig. 6. Diffraction plane of nanomaterials
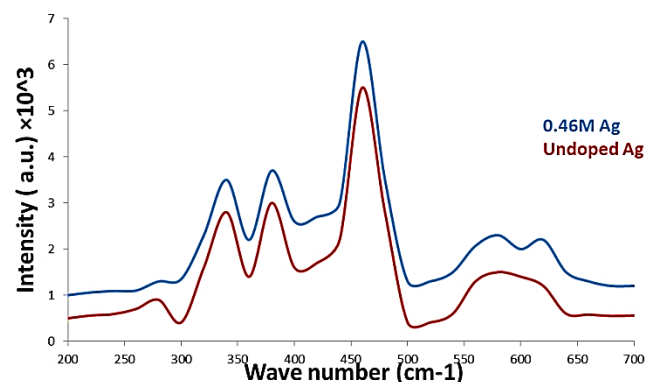
Fig. 7. Raman spectra of (a) TiO$_2$/MWCNT (b) 0.46 M Ag doping on TiO$_2$/MWCNT, Calcination temp: 400 ^{0}C, time of calcination: 16 h (color online)

4.6. Photoluminescence spectra

The photoluminescence (P.L.) spectrum is beneficial in studying the amount of disorder to measure the purity and crystalline quality. Fig. 8 reveals the structural distribution of undoped and the samples doped with 0.46 M of Ag over TiO$_2$/MWCNT. The peak of undoped and doped samples is found at the exact location and same place at 360 nm (U.V. visible regime), and another peak at 480 nm (blue/green) regime. These peaks are attributed to the intrinsic defects in the titanium dioxide crystal.
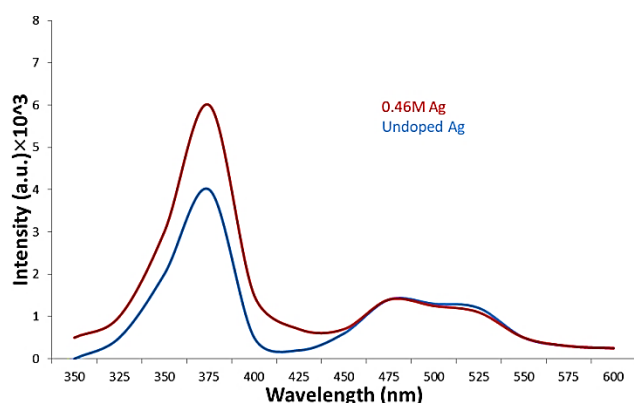
Fig. 8. PL spectra of (a) TiO$_2$/MWCNT (b) 0.46 M Ag doping on TiO$_2$/MWCNT, Calcination temp: 400 ^{0}C, time of calcnation: 16 h (color online)

4.7. Electrical properties

4.7.1. Photovoltaic properties of DSSC

Photovoltaic performance was studied using a solar radiator of intensity 100 mW/cm^2; AM 1.5 G. Fig. 9 depicted a graph of current density taken on the y-axis and photovoltage taken on the x-axis.
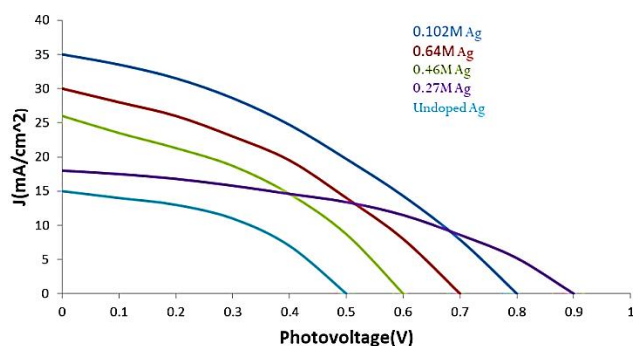
Fig. 9. Current density versus photovoltage obtained for DYSC (a) TiO$_2$/MWCNT (b) 0.27M Ag doped TiO$_2$/MWCNT (c) 0.46 M Ag doped TiO$_2$/MWCNT (d) 0.64 M Ag doped TiO$_2$/MWCNT (e) 0.102 M Ag doped TiO$_2$/MWCNT (color online)

With the help of Fig. 9 that the current density values for samples doped with 0.102 M Ag were more than those doped with 0.64 M, 0.46 M, and 0.27 M Ag. We can also be observed that with an increase in molar ratios, the current density increase because the value of the energy bandgap rose at a higher concentration of dopant (0.102 M Ag) when dopant was incorporated into TiO$_2$ coated on MWCNT and might hinder the electron transition.

Table 2 summarizes the different electrical parameters of solar cells using equations (4) and (5).

The equation efficiency of the DSSC is given by

$$\eta\% = FF \times J_{sc} \times V_{oc}/P_i \qquad (4)$$

J$_{sc}$ is the current density at short-circuit, F.F. is the fill factor, V$_{oc}$ is the potential at the open-circuit, and P$_i$ is the input power of a standard solar cell. Fill factor, open circuit voltage, and current density were co-related with equation (5) given by

$$FF = J_{max\,x}\,V_{max}/J_{sc}\,x\,V_{oc} \qquad (5)$$

J$_{max}$ and V$_{max}$ represent maximum current density and maximum potential corresponding to output power so obtained. Current and voltage were measured using a Keithley meter.

Table 2. Efficiency of DYSC for (a) TiO$_2$/MWCNT (b) 0.27 M Ag doped TiO$_2$/MWCNT (c) 0.46 M Ag doped TiO$_2$/MWCNT (d) 0.64 M Ag doped TiO$_2$/MWCNT (e) 0.1021 M Ag doped TiO$_2$/MWCNT

% Ag content (M)	IPCC Peak (%)	J$_{SC}$ (mA/cm²)	VOC (volt)	F	η(%)
0	67	15.0	0.8	0.20	1.52
0.27	70	17.5	3.0	0.25	5.06
0.46	73	26.1	5.5	0.29	5.22
0.64	75	30.0	7.0	0.45	6.95
0.102	80	35.0	9.0	0.35	5.12

We can find from Table 2 that the current increases with the increase of doping concentration. Its value for undoped TiO$_2$ is found to be 15 mA/cm^2, while for sample doped with 0.27 M, 0.46 M and 0.102 M are respectively found to be 17.5 mA/cm^2, 26.1 mA/cm^2, 30 mA/cm^2 and 35 mA/cm^2. The trend of the other values, like open circuit voltage, also follows the same pattern. The increase in short-circuit current is due to the increase in dye adsorption and decrease in the charge-transfer resistance at the interface of TiO$_2$/MWCNT.

The 0.64 M Ag-doped nanocomposites showed a maximum efficiency of 6.95%, larger than undoped TiO$_2$. Moreover, with an increase in doping concentration, the photoelectrode harvesting efficiency is slowly increased and becomes highest with 0.64 M Ag-doped TiO$_2$/MWCNT; and after that, with further doping with Ag, photoelectric conversion efficiency decreases. This

result is incompatible with the development evaluated from UV-Vis and XRD spectra. The deposition of silver on the synthesized material not only shifted the Fermi level close to TiO_2 rather considerable number of electrons was also available on it [27-28]. Thus a maximum efficiency of 6.95% was obtained for our synthesized cell.

4.7.2. The IPCE Spectra of TiO₂-based DSSC

Fig. 10 depicted the IPCE spectra plotted in the wavelength range of 350-800 nm. IPCE is expressed in %, and it is given by

$$IPCE (\%) = 1240 \times J_{sc}/\lambda P_i$$

It is clear from Fig. 10 that our synthesized solar cell works on the visual side of the electromagnetic spectrum by accepting energy from dye to TiO_2/MWCNT through Ag, which enhances its photovoltaic properties. The value of IPEC varied between 65%-80% for all the samples. IPCE (%) value is large for the sample doped with 0.102 M Ag than that of undoped and even for the sample doped with 0.27 M Ag, 0.46 M Ag, and 0.64 M Ag. The higher value IPCE confirms that the sample doped with 0.102 M Ag can collect photo-excited electrons fast. It seems that it has a fast electron transfer capability and a more rapid dye absorption tendency than the other samples. The open-circuit voltage and short-circuit photocurrent density for the 0.102 M Ag-doped sample are also higher than the other samples. The optimum value of IPEC was associated with the anatase frameworks of TiO_2 (XRD: Fig. 2), high area to volume ratio of TiO_2 nanoparticle (TEM; Fig. 4 and Fig. 5), and of course, depend on the reduced bandgap energy of Ag-doped TiO_2/MWCNT nanocomposite (UV-Vis, Fig. 3). The higher value of these electrical parameters confirms that our synthesized DSSC that contain Ag-doped TiO_2/MWCNT have the strong potential of sensitivity. All these parameters jointly contributed to the improved performance of our synthesized solar cell [29].
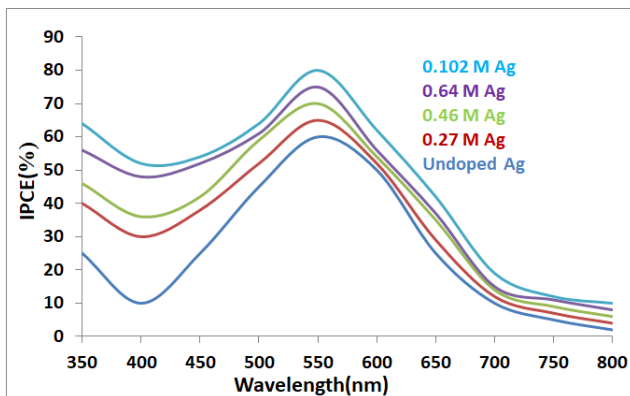
Fig. 10. IPCE spectra obtained for (a) Undoped (b) 0.27 M Ag doped TiO₂/MWCNT (c) 0.46 M Ag doped TiO₂/MWCNT (d) 0.64 M Ag doped TiO₂/MWCNT (e) 0.102 M Ag doped TiO₂/MWCNT (color online)

4.8. EIS analysis

Electrochemical impedance spectroscopy (EIS) is an outstanding new technique related to the interfacial polarization of materials to be investigated [15]. The plot is found to be semi-circular. We can study about grain and grain boundary of the synthesized material using this plot. EIS reveals that every semi-circular plot can be regarded as a practical circuit containing a resistance (R) and a capacitance (C) connected in a parallel. The real and imaginary parts of complex impedance are represented by

$$Z^* = Z' + jZ'' \qquad (6)$$

Fig. 11 represents the Nyquist plot of our synthesized cell. The equivalent series resistance of the cell is given by the coupling of the high-pitched semi-circles on the x-axis. The series resistance depends on concentrations of Ag used as the photoanodic material. We can find two semi-circles in Fig. 11. This figure also confirms that the internal resistance of our synthesized solar cell under the above condition is 22 ohms.

At more minor frequencies, the complex impedance values are more significant, which explains the heavier polarization [21]. The impedance decrement is due to the electrons' considerable mobility at TiO_2/ MWCNT. Thus the fabricated material may serve as a pathway in the transfer of electrons quickly and swiftly [29-31].
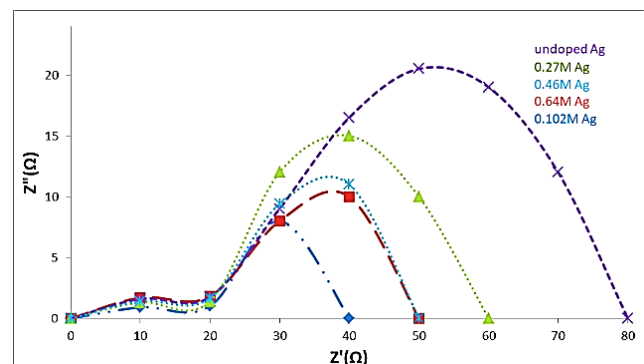
Fig. 11. Nyquist plot obtained for (a) TiO₂/MWCNT (b) 0.27 M Ag doped TiO₂/MWCNT (c) 0.46 M Ag doped TiO₂/MWCNT (d) 0.64 M Ag doped TiO₂/MWCNT (e) 0.102 M Ag doped TiO₂/MWCNT (color online)

5. Conclusion

In this study, Ag nanoparticle was doped onto TiO_2/MWCNT and synthesized material was used as photoanodic material to fabricate our solar cell. We have discussed here in detail the performance and long-term stability of our solar cell. In parallel, in this study, we have tried the electrical factors responsible for influencing the cell's efficiency values. The efficiency of our synthesized solar cell is found to be 6.95% up to 1000h of the continuous use of our solar cell. The valuable observation that we got from the synthesis of our cell is that the

internal resistance of the electrolyte of the cell is only 22 ohms.

References

[1] M. Ni, M. K. H. Leung, D. Y. C. Leung, K. Sumathy, Renewable and Sustainable Energy Reviews **11**(3), 401 (2007).

[2] J. Liqiang, S. Xiaojun, X. Baifu, W. Baiqi, C. Weimin, F. Hongganga, J. Solid State Chem. **177**, 3375 (2004).

[3] A. K. A. Gafoor, J. Thomas, M. M. Mustafa, J. Electron. Mater. **40**, 2152 (2011).

[4] O. Legrini, E. Oliveros, A. M. Braun, Chem. Rev. **93**, 671 (1993).

[5] T. Sugimoto, X. Zhou, A. Muramatsu, J. Colloid Interface Sci. **252**, 347 (2002).

[6] B. Jin, X. Zhou, X. Xu, L. Ma, Z. Wu, Y. Huang, World J. Nano Sci. Engg. **3**, 1 (2013).

[7] S. J. Tauster, S. C. Fung, R. L. Gaster, J. Chem. Sc. **100**, 170 (1978).

[8] M. H. Manarola, B. H. Parmar, A. S. Pillai, V. S. Joshi, Multi-Disciplinary Edu Global Quest **1**(4), 138 (2012).

[9] T. Prodromakis, C. Papavassiliou, Appl. Surf. Sci **255**, 6989 (2009).

[10] Hyun-Jun Hwang, Hak-Sung Kim, J. Composite Materials **49**(14), 1679 (2014).

[11] Y. Dong, X. Wang, E. Jin, S. Jeong, B. Jin, S. Lee, Renewable Energy **135**, 1207 (2019).

[12] Khalil Ebrahim Jasim: "Dye-sensitized solar cells-working principles, challenges, and opportunities" Chapter in; Leonid A. Kosyachenko (ed), Solar Cells-Dye- Sensitized Devices, Intech open (2011).

[13] Gabriela G. Sonai, A. Tihonan, K. Miettunen, D. Peter, F. Ana, J. Phys. Chem. C. **121**, 17577 (2017).

[14] S. Mazumdar, Ying Zhao, Xiaodan Zhang, Review Articles. Front. Elect. Opt. Elect. 2021.

[15] Jan Lucas, S. M. Dolter, B. Brockhagen, E. T. Gothe, Crystals **10**, 1158 (2020).

[16] Hyun-Jun Hwang, Hak-Sung Kim, J. Comp. Materials **48**(14), 169 (2014).

[17] Chih-Hung Tsai, Chia-Ming Lin, Yen Chenng Liu, Internet Archive **10**, 195 (2020).

[18] Xinyu Zhang, Jiaqian Qin, Yanan Xue, Pengfei Yu, Bing Zhang, Limin Wang, Riping Liu, Scientific Reports 4, Article number: 4596 (2014).

[19] J. Qi, X. Dang, P. T. Hammond, A. M. Belcher, ACS Nano **5**(9), 7108 (2011).

[20] G. W. Lee, S. J. Kumar, Phys. Chem. B **109**, 17128 (2005).

[21] Y. W. Wang, L. Zhang, S. Li, P. Jena, J. Phys. Chem. C **113**, 9210 (2009).

[22] H. Serier, M. Gaudon, M. Menetrier, Solid State Sci. **11**(7), 1192 (2009).

[23] V. Stengl, S. Bakardjieva, N. Murata, Mater. Chem. Phys. **114**, 217 (2009).

[24] V. Stengl, S. Bakardjieva, J. Phys. Chem. C. **114**, 19308 (2010).

[25] L. G. Devi, N. Kottam, S. G. Kumar, J. Phys. Chem. C. **113**, 5593 (2009).

[26] Y. W. Wang, L. Zhang, S. Li, P. Jena, J. Phys. Chem. C. **113**, 9210 (2009).

[27] Su Pei Lim, A. Pandikumar, H. Lim, R. Ramasamy, N. Huang, Physical Chemistry Chemical Physics **19**(2), 11922 (2017).

[28] Jinghua Hu, Jiejie Cheng, S. Tong, Y. Yang, Inter. J. Photoenerg. Annual Report (2016).

[29] K. Farzaneh, R. M. Mansour, H. Hassan, J. Alloys and Comp. **890**, 161709 (2021).

[30] A. A. Saif, Z. Ajamal, Z. Sauli, P. Poopalan, Mat. Sc. (Medziagotyra) **17**, 186 (2011).

[31] T. Prodromakis, C. Papavassiliou, Appl. Surf. Sci. **255**, 6989 (2009).

[32] S. Faizah, F. Taaseen, S. Ahmad, G. William, M. Messer, S. Viji, A. J. Saleh, M. Subhan, M. Jamaluddin, Molecules **25**, 4021 (2020).

[*]Corresponding author: mujahidm72@gmail.com